EFFECTS OF MANUFACTURING VARIABILITY ON MODEL-BASED CT IMAGE RECONSTRUCTION

J. W. Eberhard, K. H. Hedengren and M. L. Hsiao

Corporate Research and Development Center
General Electric Company
Schenectady, NY 12301

INTRODUCTION

In recent years, x-ray Computed Tomography (CT) imaging has become much more widely used in industrial applications. In many such applications, however, only incomplete data sets [1] are available, and image quality is degraded by the absence of complete data. In this paper, a model-based CT reconstruction technique for enhancing incomplete data CT image quality is presented. A two-dimensional registration method which will ensure proper utilization of a priori information from CAD model is introduced. Images are shown to demonstrate manipulator position variability as well as blade to blade variability. Variability is quantified by the translation and rotation factors used in geometric transformation. In addition, incomplete data CT image simulation results are presented which show the effects of manufacturing variability on flaw detectability in these images.

MODEL-BASED CT RECONSTRUCTION

The use of a priori information from solid models is a powerful technique for enhancing the quality of incomplete data CT images. Several techniques have been developed to incorporate CAD model information into limited angle CT reconstruction to improve image quality. In the projection data approach [2,3], projection data acquired over the available angular range and projection data calculated from the model image over the missing angular range are used for reconstruction. In the iterative reconstruction approach [2,4], projection data is again acquired over the available angular range, and a limited angle image is reconstructed from this data. Three types of a priori information are then applied to the limited angle image: 1) pixels are non-negative, 2) pixels are less than some maximum value, and 3) pixels outside the object are zero. The corrected limited angle image is then used to calculate the projection data in the missing angular range. This procedure is iterated as often as necessary to achieve a high quality image. In the image processing and analysis approach [2], the limited angle reconstruction error is added to the limited angle image, reconstructed from projection data acquired over the available angular range, to arrive at the best part image. The limited angle reconstruction error is constructed by subtraction and normalization of the complete CT image, reconstructed from the projection data calculated from the model over the full angular range, and the limited angle CT image, reconstruction from the projection data calculated from the model over the available angular range.
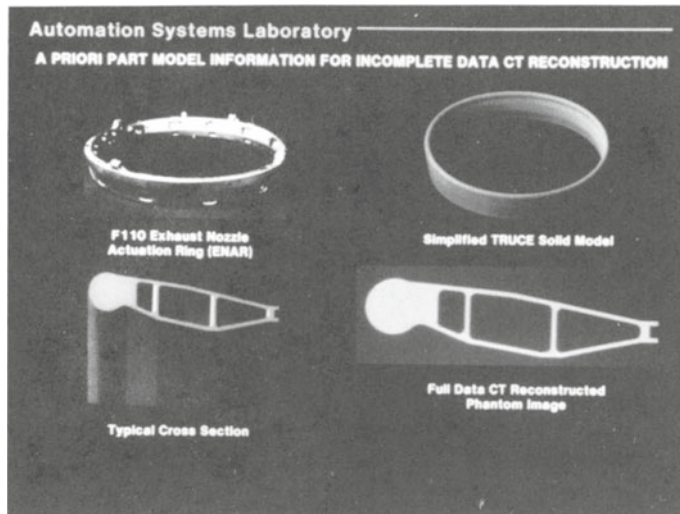
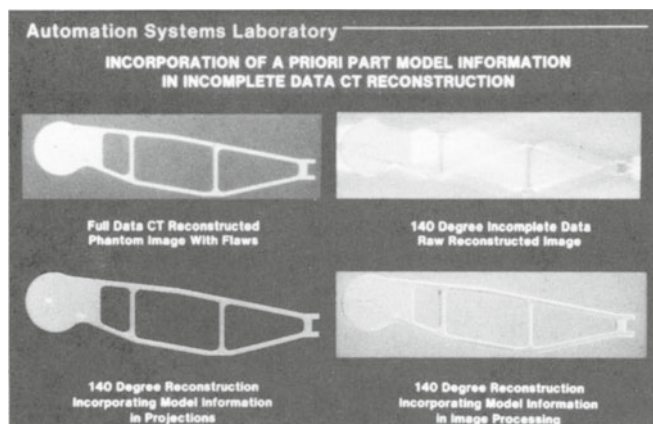Figure 1. F110 Exhaust Nozzle Actuation Ring (ENAR)

Figure 2. Projection Data Approach and Image Processing and Analysis Approach

The part chosen for model based CT inspection and analysis is the Exhaust Nozzle Actuation Ring (ENAR) from the GE F110 aircraft engine shown in Fig. 1a. A simplified CAD model was created, in which the most complex cross-section was simply rotated into a cylinder of revolution. The cross-sectional model is shown in Fig. 1b, and the full model is shown in Fig. 1c. A two dimensional CT image of this cross-section (6.9" high and 1.9" wide) derived from the model is shown in Fig. 1d. The model provides the basic part geometry information, and the image derived from this geometry is referred to as the Model Image. An image with three flaws incorporated into the exact part geometry was also created, and this image is referred to as the Simulated Part Image. The first flaw is a localized elliptical void roughly 5 pixels long and 3 pixels high (actually 17 total pixels), the second flaw is an 88% dense microshrink region covering a 131 pixel ellipse (roughly 9 pixels high and 17 pixels wide), and the third flaw is a crack 7 pixels long and 2 pixels wide (14 total pixels). The results using the projection data approach and the image processing and analysis approach on a limited angle image based on 140 degrees of available data are shown in Fig. 2. The improvement in image quality is substantial and all flaws are clearly reconstructed.
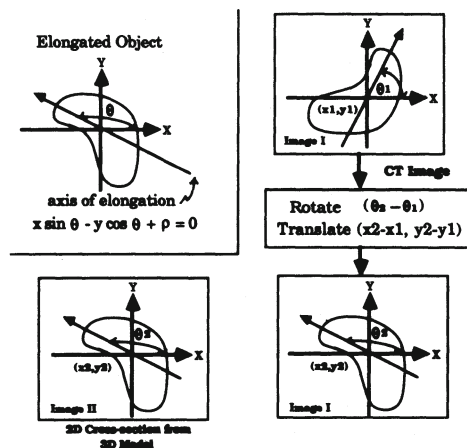
Figure 3. Registration Based on Moments

REGISTRATION BASED ON MOMENTS

In order to properly utilize a priori information from a CAD model for limited-angle CT reconstruction, accurate registration between the model image and the CT image is required. A two-dimensional registration method based on the first and second moments is used. Figure 3 shows a CT image reconstructed from projection data and a 2-D cross section image extracted from solid model with different position and orientation. A geometric transformation is applied to the CT image such that the resultant image is geometrically correlated to the 2-D cross section image. The translation factor is estimated from the offset of the object central gravity point, which can be computed as the first moment about the x and y axes. The rotation is computed from the variations of the orientation angle. The axis of elongation, defined as the line for which the integral of the square of the distance to points in the object is a minimum, is used to represent the object orientation. The orientation angle is the angle between the axis of elongation and the x axis. This angle can be computed as function of the second moments about the central gravity point. A transformation matrix contains both the translation and rotation factors are indicated as follows :

$$
\begin{aligned}
T &= Rotate(z, \theta) \ \ Trans(x_0, y_0, 0) \\
&= \begin{vmatrix}
\cos\theta & -\sin\theta & 0 & x_0 \\
\sin\theta & \cos\theta & 0 & y_0 \\
0 & 0 & 1 & 0 \\
0 & 0 & 0 & 1
\end{vmatrix}
\end{aligned}
\tag{1}
$$

The translation vector $(x_0, y_0, 0)$ is estimated based on the offset of the object central gravity points. The center of mass is defined as the point where all the mass of the object could be concentrated without changing the first moment of the object about any axis. In the two-dimensional case, the central gravity point is computed as the first moment about the x and y axes. The characteristic function b(x,y) associated with each pixel p(x,y) has a value 1 for a pixel belonging to the object and a value 0 otherwise. The central gravity point of the object can be calculated as :

$$
\overline{x} = \frac{1}{area} \int\int_I x \ b(x,y) \ dx \ dy = \frac{1}{area} \sum_{(x,y)\in object} x
$$

$$
\overline{y} = \frac{1}{area} \int\int_I y \ b(x,y) \ dx \ dy = \frac{1}{area} \sum_{(x,y)\in object} y
$$

where

$$area \quad = \int \int_I \ b(x,y) \ dx \ dy \quad = \sum_{(x,y)\in object} 1 \tag{2}$$

The rotation factor can be estimated from the variation of the object orientation angle. The orientation angle θ is defined as the angle between the x axis and the elongation axis and is measured counterclockwise. For an elongated object, as shown in Fig. 3, the axis of the elongation is defined as the line for which the integral of the square of the distance to points in the object is a minimum. Suppose the line which indicates the elongation axis is stated as

$$x \sin\theta - y \cos\theta + \rho = 0 \tag{3}$$

For any pixel p(x,y) belong to the object, there exists a pixel p(x',y') belong to the axis of elongation such that the line between p(x,y) and p(x',y') is perpendicular to the elongation axis. The position of the pixel p(x',y') can be computed by solving the following simultaneous linear equations and yields :

$$\begin{cases} x' = -\rho \sin\theta + s \cos\theta \\ y' = \rho \cos\theta + s \sin\theta \end{cases} \tag{4}$$

For a pixel p(x,y) belonging to the object, r(x,y) is used to denote the perpendicular distance from the pixel p(x,y) to the elongation axis and is equivalent to the distance between the pixel p(x,y) and the pixel p(x',y'). The orientation angle θ can be estimated by minimizing the integral of the square of the distance r(x,y) which is denoted as E in Eq. (5).

$$\begin{aligned} E &= \int \int_I \ r(x,y)^2 \ b(x,y) \ dx \ dy \\ &= \int \int_I \ \{(x-x')^2 + (y-y')^2\} \ b(x,y) \ dx \ dy \\ &= \int \int_I \ (x \sin\theta - y \cos\theta + \rho)^2 \ b(x,y) \ dx \ dy \end{aligned} \tag{5}$$

Since the axis of elongation also passes through the central gravity point $(\overline{x},\overline{y})$, the variable $\rho = \overline{y} \cos\theta - \overline{x} \sin\theta$ results. Equation (5) can then be simplified as

$$\begin{aligned} E &= \int \int_I \ [(x-\overline{x}) \sin\theta - (y-\overline{y}) \cos\theta]^2 \ b(x,y) \ dx \ dy \\ &= A \ sin^2\theta - B \ \sin\theta \cos\theta + C \ cos^2\theta \end{aligned} \tag{6}$$

where A, B, and C are the second moments given by

$$\begin{aligned} A &= \int \int_I \ x^2 \ b(x,y) \ dx \ dy - \overline{x}^2 \\ B &= 2 \ \{\int \int_I \ xy \ b(x,y) \ dx \ dy - \overline{x} \ \overline{y}\} \\ C &= \int \int_I \ y^2 \ b(x,y) \ dx \ dy - \overline{y}^2 \end{aligned} \tag{7}$$

Finally, we can now address the minimization of Eq. (6). Differentiating with respect to θ and setting the result to zero leads to

$$\theta = \frac{1}{2} tan^{-1}\{\frac{B}{A-C}\} \tag{8}$$

Table 1. Manipulator Position Variation

Slice #	$\overline{x}$	$\overline{y}$	θ
1	248.714643	229.665078	-57.128429
2	240.210802	229.690102	-57.099445
3	248.594358	236.643681	-56.715534
4	237.821198	234.945839	-57.343159
5	238.824240	238.907766	-57.258156
6	248.699804	239.618062	-57.411354
7	246.756320	234.321143	-57.451622
8	241.171940	227.696537	-56.728306
9	249.386362	241.143081	-57.459347
Average	244.464432	234.736816	-57.177261
Standard Deviation	4.563325	4.556722	0.272214

MANUFACTURING VARIABILITY EVALUATION

Application of model-based CT reconstruction techniques to real parts requires that manufacturing variability be taken into consideration. It is important to know just how much nominally identical objects differ from each other due to the manufacturing process as well as the manipulator position variability. CT images have been created of several different turbine blades of the same type at identical vertical positions to demonstrate manipulator position variability as well as blade to blade variability. These images have been processed to extract exterior boundaries of the blades as well as boundaries of internal cavities in the blades. The image which results from superimposing the boundaries of the CT images on top of each other, shown in Fig. 4a, illustrates the manipulator position variations. By comparing the boundary images, measurements can be made to quantify variability both of blade position and of blade construction. Registration techniques, based on the first and second moments, are used to remove the effects of blade positional variation. Applying the registration method mentioned early, the first moment about the x and y axes as well as the orientation angle are extracted from each CT image. The translation and rotation factors are used to evaluate the effects of manufacturing variability and used for geometric transformation. Table 1 lists those values calculated from nine CT images. The average and standard deviation of the first and second moments are also presented. Geometric transformation, using the calculated $(\overline{x}, \overline{y})$ and θ, is applied to each CT image. Fig. 4b shows the results of superimposing nine CT images after registration. It is shown that the effects of manipulator variation are removed. The resultant image indicates the blade to blade variation due to manufacture processing.

EFFECTS OF MANUFACTURING VARIABILITY ON FLAW DETECTABILITY

The results in Fig. 2 were obtained for the case in which the Model Image and the Simulated Part Image are identical except for the presence of flaws in the Simulated Part Image. In any real inspection situation, manufacturing tolerances will cause actual parts to vary somewhat from the blueprints. These variations must be taken into account in any realistic inspection scheme. The initial approach which was chosen to take these variations into account was to vary the size of the Model Image relative to the size of the Simulated Part Image before using the Model Image as a mask in the Projection Data Approach and the Iterative Reconstruction Approach described above.
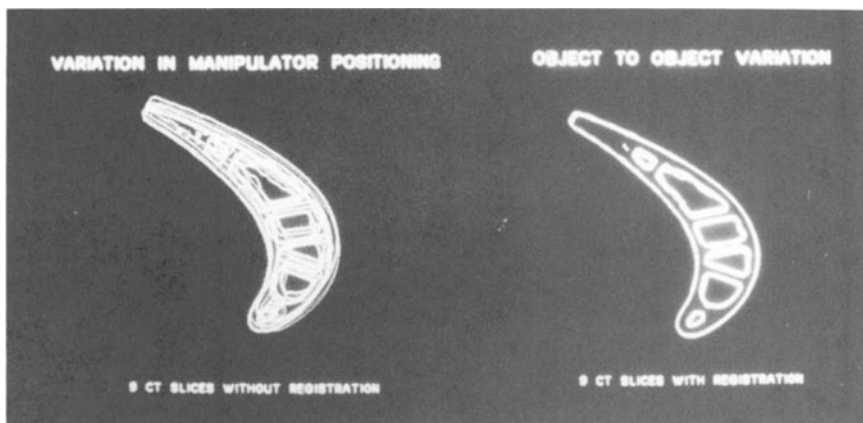
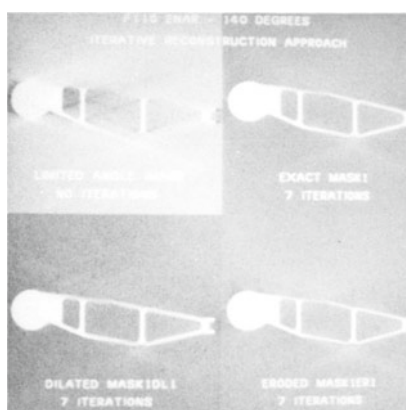Figure 4. Manipulator Positioning Variation and Blade to Blade Variation

Figure 5. Iterative Reconstruction Approach for Various Masks

Several masks were used at various stages in the analysis. These masks were derived from the Model Image by thresholding, erosion, and dilation. Thresholding creates a binary image, which can then be expanded by one (or more) pixels at the boundary (dilation), or shrunk by one (or more) pixels at the boundary (erosion). The pixel values in the Model Image range from 0. to 100., with only boundary pixels varying from the two values stated. MASK1 was created by thresholding the Model Image at a pixel value of 1. and setting all pixels above the threshold equal to 1 and all pixels below the threshold equal to 0. MASK1DL1 AND MASK1DL2 were created from MASK1 by dilating once and twice respectively, and MASK1ER1 and MASK1ER2 were created from MASK1 by eroding once and twice respectively. The masks therefore all maintain the same general shape as the Model Image, but the size varies.

Image quality as judged by the operator is essentially independent of variations in the mask size, as in shown in Fig. 5, which shows a comparison of images after 7 iterations of the iterative reconstruction technique using the exact mask and the once dilated and eroded masks. In all cases, image quality is substantially improved compared to the case where no a priori information is used (compare Fig. 5a to parts b, c, and d). Quantitative performance comparisons are required to evaluate the effects of these changes.

For voids and microshrink, the key issue is to determine whether the flaw is detectable based on its contrast with background material. In order to assess this detectability, evaluation
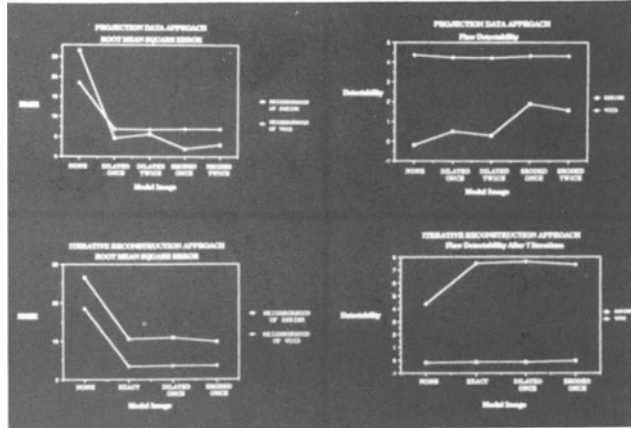
Figure 6. RMS Error and Flaw Detectability

of mean signal level, standard deviation, and Root Mean Square (RMS) Error compared to an ideal image in key regions of the image are required. For the analysis which follows, four regions have been chosen. The first region (VOID) covers the 17 pixel void in the F110 ENAR image. A companion region (VOIDNH) includes the nearest 131 pixels surrounding the void. Similarly, for the microshrink flaw, the first region (SHRINK) covers the 131 pixel defect and companion regions includes the nearest 131 pixels surrounding the microshrink region (SHRINKNH). The mean, standard deviation, and RMS Error were calculated in each region. In addition, a detectability parameter[5]

$$D = \frac{(\overline{P} - \overline{Q})}{\sqrt{\sigma_P^2 + \sigma_Q^2}} \tag{9}$$

was evaluated for each flaw and used to compare the various approaches. In Eq. 9, $\overline{P}$ and σ_P are the mean and standard deviation in the region of the flaw, and $\overline{Q}$ and σ_Q are similar values in the neighborhood of the flaw.

Consider first the detection of voids and microshrink using the projection data approach. The RMS Error in the regions VOIDNH and SHRINKNH are plotted in Fig. 6a. The point labeled NONE corresponds to the 140 degree limited angle image with no a priori information, while the other four points correspond to eroded and dilated images as indicated. Note the dramatic reduction in RMS Error as soon as any a priori information is used, and the relatively slight variation with mask size. The detectability parameter defined in Eq. 9 is plotted in Fig. 6b for these same images. Note that the detectability of the microshrink region is substantially enhanced with inclusion of a priori information, but the void region is not. Microshrink detectability is enhanced due to reduction of artifact in the image, while void detectability is essentially unaffected since the void is a high contrast flaw and incomplete data artifact is small compared to the flaw signal. Indeed, void contrast is not improved by the Projection Data Approach, since missing angle data is taken from the Model Image which contains no flaw. In general, void detectability is good and relatively independent of mask size. Shrink detectability is generally fair, and somewhat better for smaller masks than for larger ones.

Similar plots of RMS Error and Flaw Detectability are presented in Fig. 6c and d for the Iterative Reconstruction Approach using 7 iterations. Results are similar, with a few exceptions. Again, significant improvement is achieved after use of a priori information, and the amount of improvement is relatively independent of mask size. Note that using this method,

the detectability of voids is improved with iterations, but microshrink detectability remains poor. In this case, void contrast is improved with processing, since information about the void is indeed present in the images at each step of the processing, and the iterations improve the quality of information at each step. Microshrink detectability, however, is relatively poor, even after iterations, which reflects the relative inability of this method to remove the steaking artifacts characteristic of limited angle CT images.

In conclusion, both the projection data approach and the iterative reconstruction approach provide significant improvements (factors of 3 to 10 or more) in incomplete data image quality. The Projection Data Approach provides greater improvement for microshrink detection while the Iterative Reconstruction Approach provides greater improvement for void detection.

SUMMARY

Model-based approaches have been proved as a powerful technique for enhancing the incomplete data CT image quality. A registration method, based on the first and second moments, has been developed and used to remove the effects of positional variation. This technique will ensure proper utilization of CAD model information. The effects of manufacturing variabilities have been evaluated based on the translation and rotation factors used to do geometric registration. In addition, incomplete data CT image simulation results show that typical effects of manufacture variability occurring in practice (at least in turbine blades) do not degrade flaw detectability using model based CT reconstruction techniques. It is concluded that the model-based approaches provide significant improvement in incomplete data image quality.

REFERENCE

1. Stark, H., ed. Image Recovery: Theory and Application, Academic Press, Inc., Orlando, 1987. Ch. 2, 9, and 11.

2. Eberhard, J.W. and Hedengren, K.H., "Use of A Priori Information in Incomplete Data X-Ray CT Imaging", in Review of Progress in Quantitative Nondestructive Evaluation, edited by D. O. Thompson and D. E. Chimenti (Plenum Publishing Corporation, New York, 1988), Vol. 7A, pp. 723-730.

3. Eberhard, J.W. and Tam, K.C., "Incomplete Data CT Imaging", presented at 1988 ASNT Spring Conference, April 11-15, Orlando, Fla.

4. Tam, K.C. and Perez-Mendez, V., "Tomographic Imaging with Limited Angle Input", J. Opt. Soc. Amer., Vol. 71, pp. 582-592. (1981)

5. Jennings, R., "Fundamental Limits on Performance of Imaging Systems", presented at Fall Meeting, New York State Section, American Physical Society, Physics of Medical Imaging Symposium, October 4-5, 1985, Schenectady, New York, 1985.